FreeHydroCells

D1.3

Report on the electrical and optical characterisation and the photoelectrochemical analysis of TMD/TCO pn-junctions in the dark and under different illumination and different electrolyte pH conditions, version I

WP1 TMD/TCO Materials: Materials and Processing Development and Characterisation

Status: Final

19 December 2024

Funded by the European Union

Document Information

Title	Report on the electrical and optical characterisation and the photoelectrochemical analysis of TMD/TCO pn-junctions in the dark and under different illumination and different electrolyte pH conditions, version I
Dissemination Level	Public
Deliverable Leader	UCC
Type	R - Document, report
Contributing Authors (Name, Organisation)	Ailbe Ó Manacháin (UCC), Anna Power (UCCAC), Jun Lin (UCC), Salvatore Antonino Lombardo (CNR), Ulrich Plachetka (AMO), Vikas Jangra (RWTH)

Funding

This project has received funding from the European Union under grant agreement No 101084261.

Disclaimer

Table of Contents

Executive Summary 3
0. Introduction 4
1. Task 1.4: Electrical and Optoelectronic Characterisation of the TCOs and TMDs 8
1.1 Introduction 8
1.2 Electrical and Optoelectronic Results and Discussion 8
2. Task 1.5: Photoelectrochemical Characterisation of the TCOs and TMDs 13
2.1 Introduction 13
2.2 Photoelectrochemical Results and Discussion 13
3. Conclusions and Perspectives 17
Appendices 18
Appendix 1: List of acronyms 18

Executive Summary

The effect of climate change on the Earth has become critical. We must find a way to reduce and ultimately replace the necessity for burning fossil fuels to extract our energy needs, in order to reduce the level of pollutants from such processes entering the atmosphere and driving global warming with the related negative consequences for the environment and humanity globally. Many “green” energy conversion solutions (with no pollutant byproducts) have been investigated to date, including wind, wave and solar. Significant bottlenecks in achieving high conversion efficiency, low-cost production and operation, low maintenance cost, long and stable product life, energy storage and material sustainability have significantly reduced the ability of these potentially green solutions to challenge – practically, energetically and financially – the dominant and pollutant-rich fossil fuel energy extraction methods.

The FreeHydroCells project is designated by the European Commission as a high risk–high reward (if fully successful) project that has very specific objectives aimed at addressing these top-level bottlenecks, by adopting a radical and novel approach of employing environmentally-benign sustainable materials to form a stable, high-efficiency/low-cost, water splitting system driven by sunlight absorption in a buried multijunction cell-based system.

As we approach the end of Month M26 of M40 in the project timeline, the present deliverable report D1.3 is focused on providing a public dissemination level summary of the Work Package 1 (WP 1) results to date on the electrical, optoelectronic and photoelectrochemical characterization of the BMJ building block TCO and TMD materials, for substrates, capping layers, and for the thin film junctions themselves.

Understanding the electrical, optoelectronic and photoelectrochemical properties of the material building blocks in WP 1 plays an important part in developing the input sources for the material integration of forming multijunction material systems in WP 2 in order to form buried multijunction photoelectrochemical cells to split water and make green molecular (diatomic) hydrogen fuel. FreeHydroCells adopts an iterative (symbiotic-like) process interrelationship between the four technical Work Packages, including between WP 1 and WP 2. Therefore, understanding the electrical, optoelectronic and photoelectrochemical properties of the material building blocks not only guides the direction of activities in WP 2, it also is influenced by the feedback findings from WP 2 through our iterative loop process in the project methodology. The report covers: (1) Task 1.4 (Electrical and Optical Characterisation); and (2) Task 1.5 (Photoelectrochemical Characterisation) of WP 1.

We demonstrate that by increased development and improvement in the small-to-large area TMD and TCO layer quality, and by moving towards a many TMD/TCO junction cell, we can progressively improve the zero bias photocurrent density.

We can infer that by the continued improvement to the TMD doping and to the TMD and TCO layers, and especially with increased numbers of TMD/TCO junctions alongside the observed area increases, the zero bias photocurrent density could potentially have a trajectory towards a water splitting capability.

FreeHydroCells
UCC University College Cork, Ireland
RWTH AACHEN UNIVERSITY
Consiglio Nazionale delle Ricerche
cea
AMO
BARDS
UCC ACADEMY
Funded by the European Union

0. Introduction

The aim of all activities in WP 1 is to achieve the baseline building block component materials, structures and properties – as illustrated for TMDs in Figure 0.1.

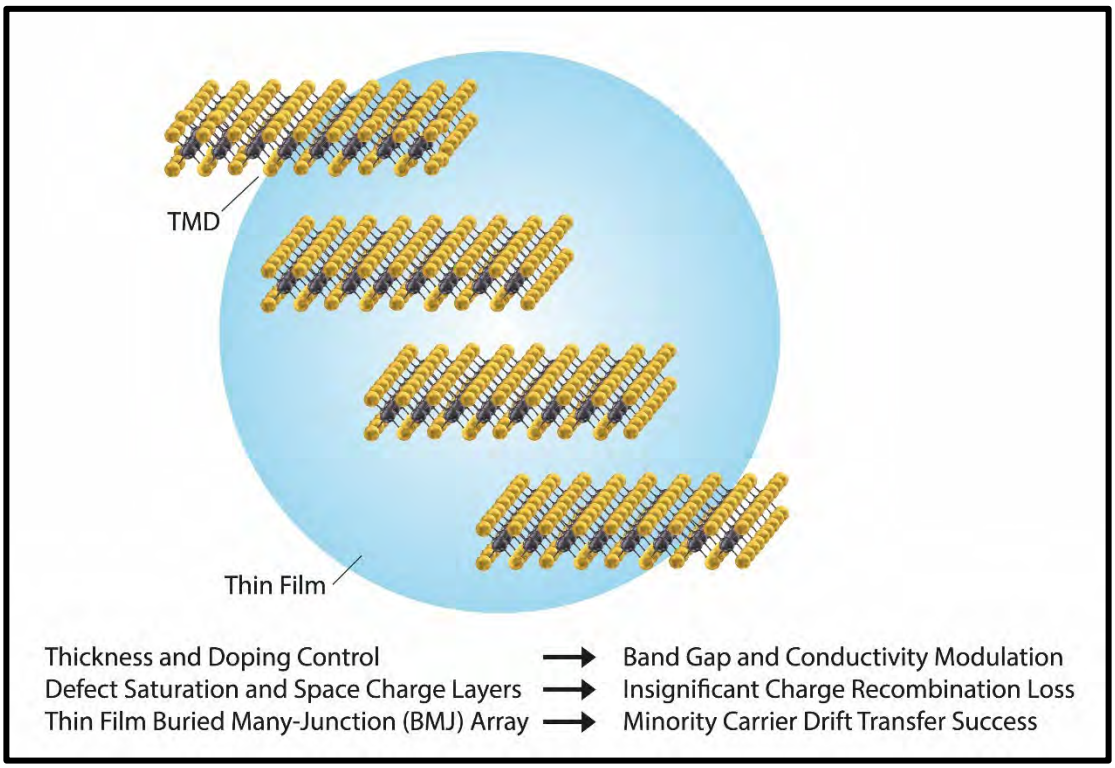

Figure 0.1: Illustrative schematic of material layer building block aims in WP 1 under Tasks 1.1-1.5 in order to enable and advance the WP 2 objectives.

The building block materials are aimed at allowing the consortium to ultimately create a fully integrated tandem PEC cell as illustrated in Figure 0.2 for large irradiation areas that will be formed in WP 2 and provided to WP 3 - WP 4 for the water-splitting system.

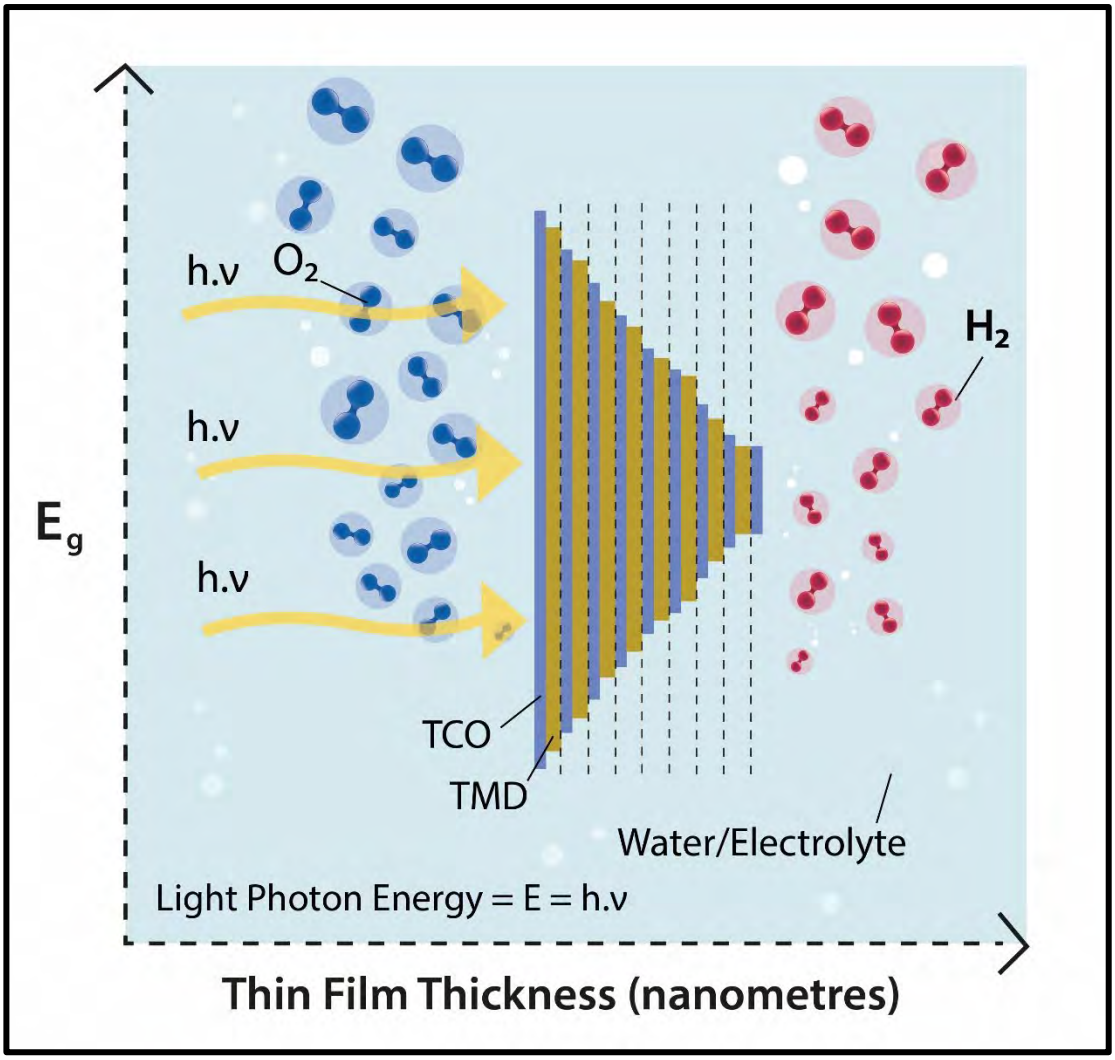

Figure 0.2: Illustrative schematic of the WP 2 objective in forming buried multijunction layers from the material building blocks of WP 1.

Tables 0.1 (from Task 1.1) and 0.2 (from Task 1.2) list the building block TCO and TMD materials, respectively, investigated in WP1 and made available to Tasks 1.4 and 1.5 of WP 1 up to M26 of M40 for investigation where applicable.

Table 0.1. TCO materials realised by the FreeHydroCells Consortium in the M1-M26 period.

Partner	TCO ID Material	Method	Substrate	Thickness Nominal (nm)	Type (NID, n, or p)
AMO	TCO-1	ALD	Glass	1-20	n
AMO	TCO-2	PVD	Glass	20-200	n
AMO	TCO-3	PVD	Glass	20	p
AMO	TCO-4	PVD	Glass	50-100	p
AMO	TCO-5	PVD	Glass	25-50	n
UCC	TCO-6	ALD	SiO2/Si	45	n
UCC	TCO-7	ALD	Sapphire	45	n
UCC	TCO-8	ALD	Quartz	45	n
UCC	TCO-9	ALD	SiO2/Si	50	p
UCC	TCO-10	ALD	Sapphire	50	p
UCC	TCO-11	ALD	Quartz	50	p

UCC	TCO-12	ALD	SiO2/Si	50	n
UCC	TCO-13	ALD	Glass	50	n
UCC	TCO-14	ALD	Glass	50	n
UCC	TCO-15	ALD	Sapphire	50	n
UCC	TCO-16	ALD	SiO2/Si	500	n
UCC	TCO-17	ALD	Glass	500	n
UCC	TCO-18	ALD	TMD/SiO2/Si	7	n
UCC	TCO-19	ALD	TMD/TCO/SiO2/Si	7	n
UCC	TCO-20	ALD	TMD/Sapphire	7	n
UCC	TCO-21	ALD	TMD/TCO/Sapphire	7	n
UCC	TCO-22	ALD	TMD/TCO/Glass	7	n
UCC	TCO-23	ALD	TMD/TCO/Glass	7	n
UCC	TCO-24	ALD	TMD/TCO/Glass	7	n
UCC	TCO-25	ALD	TMD/TCO/Glass	7	n
UCC	TCO-26	ALD	TMD/TCO/Glass	7	n
UCC	TCO-27	ALD	TMD/TCO/Glass	7	n
UCC	TCO-28	ALD	TMD/Glass	7	n
UCC	TCO-29	CVD-TAC	SiO2/Si	7	n
UCC	TCO-30	CVD-TAC	TMD/SiO2/Si	7	n
UCC	TCO-31	ALD	TMD/Sapphire	7	n
UCC	TCO-32	ALD	Glass	450	n
UCC	TCO-33	ALD	TMD/TCO/Glass	45	n
CNR	TCO-34	PVD	Glass	10-200	n
CNR	TCO-35	PVD	Glass	10-100	n
CNR	TCO-36	PVD	Glass	1-10	NID
CNR	TCO-37	PVD	Glass	1-10	NID
CNR	TCO-38	PVD	Glass	10-200	n
CNR	TCO-39	Commercial	TCO/Glass	650	n

Table 0.2: TMD materials prepared by the FreeHydroCells Consortium in the M1-M26 period.

Partner	TMD ID Material	Method	Substrate	Thickness Nominal (nm)	Type (NID, n, or p)
UCC	TMD-1	CVD-TAC	SiO2/Si	40	p
UCC	TMD-2	CVD-TAC	SiO2/Si	40	n
UCC	TMD-3	CVD	SiO2/Si	10	NID
UCC	TMD-4	CVD	TCO/SiO2/Si	10	NID
UCC	TMD-5	CVD	Sapphire	10	NID
UCC	TMD-6	CVD	TCO/Sapphire	10	NID
UCC	TMD-7	CVD	TCO/Glass	10	NID
UCC	TMD-8	CVD	TCO/Glass	10	NID
UCC	TMD-9	CVD	TCO/Glass	10	NID
UCC	TMD-10	CVD	TCO/Glass	10	NID
UCC	TMD-11	CVD	TCO/Glass	10	NID
UCC	TMD-12	CVD	TCO/Glass	10	NID
UCC	TMD-13	CVD	Glass	10	NID
UCC	TMD-14	CVD-TAC	SiO2/Si	40	NID
UCC	TMD-15	CVD-TAC	SiO2/Si	40	NID

UCC	TMD-16	CVD-TAC	Sapphire	40	NID
UCC	TMD-17	CVD-TAC	Sapphire	40	NID
UCC	TMD-18	CVD-TAC	Si	40	NID
UCC	TMD-19	CVD-TAC	Si	40	NID
UCC	TMD-20	CVD-TAC	SiO2/Si	40	n
UCC	TMD-21	CVD-TAC	SiO2/Si	40	n
UCC	TMD-22	CVD-TAC	SiO2/Si	40	n
UCC	TMD-23	CVD-TAC	SiO2/Si	40	n
UCC	TMD-24	CVD-TAC	SiO2/Si	40	n
UCC	TMD-25	CVD-TAC	SiO2/Si	40	n
UCC	TMD-26	CVD-TAC	SiO2/Si	40	p
UCC	TMD-27	CVD-TAC	SiO2/Si	40	p
UCC	TMD-28	CVD-TAC	SiO2/Si	40	p
UCC	TMD-29	CVD-TAC	Sapphire	40	n
UCC	TMD-30	CVD-TAC	Sapphire	40	n
UCC	TMD-31	CVD-TAC	Sapphire	40	n
UCC	TMD-32	CVD-TAC	Sapphire	40	n
UCC	TMD-33	CVD-TAC	Sapphire	40	n
UCC	TMD-34	CVD-TAC	Sapphire	40	n
UCC	TMD-35	CVD-TAC	Sapphire	40	p
UCC	TMD-36	CVD-TAC	Sapphire	40	p
UCC	TMD-37	CVD-TAC	Sapphire	40	p
UCC	TMD-38	CVD-TAC	Si	40	n
UCC	TMD-39	CVD-TAC	Si	40	n
UCC	TMD-40	CVD-TAC	Si	40	n
UCC	TMD-41	CVD-TAC	Si	40	n
UCC	TMD-42	CVD-TAC	Si	40	n
UCC	TMD-43	CVD-TAC	Si	40	n
UCC	TMD-44	CVD-TAC	Si	40	p
UCC	TMD-45	CVD-TAC	Si	40	p
UCC	TMD-46	CVD-TAC	Si	40	p
UCC	TMD-47	CVD	SiO2/Si, sapphire	10	NID
UCC	TMD-48	CVD	SiO2/Si, sapphire	10	p
RWTH	TMD-49	PVD-CVD-TAC	SiO2/Si, sapphire	3.8	NID, n, p
RWTH	TMD-50	PVD-CVD-TAC	SiO2/Si, sapphire	6.2	NID, n, p
RWTH	TMD-51	PVD-CVD-TAC	SiO2/Si, sapphire	8	NID, n, p
RWTH	TMD-52	PVD-CVD-TAC	SiO2/Si, sapphire	14.9	NID, n, p
RWTH	TMD-53	PVD-CVD-TAC	SiO2/Si, sapphire	4.3	NID, n, p
RWTH	TMD-54	PVD-CVD-TAC	SiO2/Si, sapphire	6.6	NID, n, p
RWTH	TMD-55	PVD-CVD-TAC	SiO2/Si, sapphire	11	NID, n, p
RWTH	TMD-56	PVD-CVD-TAC	SiO2/Si, sapphire	11.7	NID, n, p
CNR	TMD-57	Drop Casting	TCO-39/glass	1-3	p
CNR	TMD-58	Drop Casting	TCO-39/glass	1-3	p
CNR	TMD-59	Drop Casting	TCO-39/glass	1-3	p
CNR	TMD-60	Electrodeposition	TCO-39/glass	1-3	p

The growths and structural, chemical and physical assessments in Tasks 1.1-1.3 achieved the objective of confirming the formation of TCOs and TMDs, and also guided us in our building block selection process for the Task 1.4-1.5 electrical, optoelectronic and photoelectrochemical assessments.

We will show that the TCO-based activities in WP 1 included here in D1.3 have permitted a broad investigation of building block TCOs for multijunction layers, for capping layers and for use as a substrate. We will also show that the TMD-based activities in WP 1 included here in D1.3 have permitted a broad investigation of building block TMDs for multijunction absorber and pn-junction layers.

1. Task 1.4: Electrical and Optoelectronic Characterisation of the TCOs and TMDs

1.1 Introduction

Task 1.4 essentially focuses on assessing the electrical and optoelectronic behaviour of the potential material building blocks for the TCOs and TMDs multijunction layers, the TCO surface capping layers, and any potential TCO substrate developed and characterised in Tasks 1.1-1.3. It involves the partners AMO, RWTH, CNR, and UCC, with UCCAC acting in the capacity of project management, and it spans the period M1-M37 of the project 40-month timeline.

The overall focus is on low-cost, low temperature processing, and high performance, which in particular for TCOs means high optical transparency and for TMDs means high absorbance, and in both cases high electrical conductivity and the use of environmentally-benign, low-cost chemical elements, including in their delivery.

1.2 Electrical and Optoelectronic Results and Discussion

The electrical characteristics of the TCO-5 films deposited by AMO have been evaluated by UCC (See Table 1.4.1). The films deposited on glass show resistivities of the order of 1 Ohm-cm, n-type character, and relatively low carrier mobility, of the order of 0.2 cm^2/Vs. When the TCO-5 materials are deposited on TCO-4 (or TCO-5 covered by TCO-4) the apparent resistivities and mobilities increase and decrease, respectively. This may be due to the formation of a pn-junction or a heterojunction TCO-4 / TCO-5 which decreases the amount of available carriers due to the depletion layer.

Table 1.4.1: Evaluation of electrical characteristics of deposited AZO films by AMO.

Sample	Sheet resistivity (Ω/sq.)	Resistivity (Ω*cm)	Sheet carrier concentration (cm^{-2})	Carrier concentration (cm^{-3})	Carrier type	Mobility ($cm^2/V*s$)
TCO-5 d1	394k	0.98	6.86×10^{13}	2.74×10^{19}	N (100%)	0.23
TCO-5 d2	821k	4.1	3.72×10^{13}	7.45×10^{18}	N (99%)	0.20
TCO-5 d2 / TCO-4 d2	5.07M	75.98	6.40×10^{13}	4.27×10^{18}	P to N (98%)?	0.019
TCO-5 d1 / TCO-4 d1	46.90M	351.7	3.88×10^{12}	5.17×10^{17}	N (89%)	0.034
TCO-4 d2 / TCO-5 d2	76.32M	1.14k	3.57×10^{12}	2.38×10^{17}	N (100%)	0.023
TCO-4 d1 / TCO-5 d1	10.97M	82.24	1.38×10^{13}	1.84×10^{18}	N (100%)	0.041

In this period, with regard to TCOs, UCC has studied the formation of TCO films by ALD on various substrates – glass, sapphire, SiO2/Si, etc. The achieved results are extremely promising. Table 1.4.2 shows the electrical characteristics of such films by UCC. The layers are n-type, with carrier concentrations and mobilities of the order of 1E19 /cm^3 and 20 cm^2/Vs.

Table 1.4.2: Electrical characteristics of TCO and TMD layers by ALD on various substrates. "A" refers to process A, and "B" refers to process B. Such processes modify the properties of the materials to different extents.

Sample	Substrate	Sheet Resistivity (Ohm/Sq)	Resistivity (Ohm-cm)	Sheet Carrier Concentration (1/cm^2)	Carrier Concentration (1/cm^3)	Carrier Type	Mobility (cm^2/V-s)
TCO-14	c-plane sapphire	3360.00	0.016800	9.08E+13	1,82E19	N	20.46
TCO-14	Glass	4580.00	0.022900	6.37E+13	1.27E+19	N	21.40
TCO-39	Glass	6.92	0.000381	2.61E+16	4.75E+20	N	34.52
TCO-17A	Glass	33.60	0.001500	1.10E+16	2.44E+20	N	16.20
TCO-17B	Glass	501.60	0.023000	3.50E+15	7.78E+19	N	35.90
TCO-32A	Glass	13.40	0.000600	4.00E+16	8.90E+20	N	11.50
TCO-32B	Glass	47.50	0.002000	3.30E+16	7.30E+20	N	4.00
TMD-06	TCO-32A/Glass	178710.00	10.190000	7.33E+13	1.29E+18	N	0.48

Figure 1.4.1 provides the Hall-effect electrical data for the TAC-CVD doped TMDs by UCC. We can see that the properties for the WS2 samples fall largely outside the preferred zone (light red shading) for PEC cell performance, whereas the MoS2 samples – especially those that are increasingly doped, fall inside the preferred properties zone for PEC cell performance, an encouraging sign for in the latter case. The samples investigated were the non-intentionally doped MoS2 (NID, TMD-14) and 5 %, 18 % doped MoS2 (TMD-21 and TMD-25, respectively), as well as NID WS2 (TMD-15), 2 % and 4 % doped WS2 (TMD-{26,27}, respectively) TMD materials were investigated.

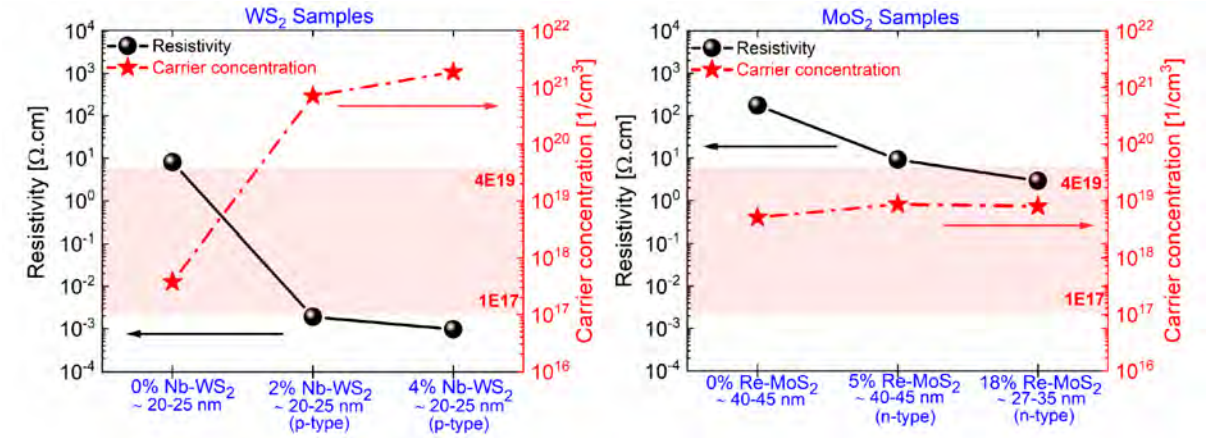

Figure 1.4.1: Hall-effect results for the TAC-CVD TMD samples by UCC. The light red zone shows the property ranges most suitable for PEC water-splitting applications. The non-intentionally doped MoS2 (NID, TMD-14) and 5 %, 18 % doped MoS2 (TMD-21 and TMD-25, respectively), as well as NID WS2 (TMD-15), 2 % and 4 % doped WS2 (TMD-{26,27}, respectively) TMD materials were investigated.

CNR has adopted photoluminescence (PL) spectroscopy to monitor MoS2 / FTO samples. In general PL can provide a powerful tool to evaluate the coupling of the pump light with the semiconductor or dielectric materials. Pump light is absorbed, usually with the formation of excitons in the case of semiconductors, and then the excitation can be relaxed radiatively, resulting in the sample photoluminescence. Therefore, the PL phenomenon in a semiconductor recalls the photovoltaic effect, so it is a powerful tool to investigate materials for photoelectrochemical cells with novel and unconventional materials. PL has been carried out at room temperature with a 533 nm laser pump light at 1 mW and 1 um spot size. Fig. 1.4.2 reports the case of MoS2 / FTO samples. Note that the spectra in the as-deposited and annealed samples (top and bottom, respectively) show noticeable differences: PL is much more intense in the annealed samples. This indicates either a better coupling of photocarriers with the MoS2 film or some MoS2 defect annealing after the thermal treatment.

The optical characterization of the MoS2 / FTO materials in CNR has also included UV-VIS-NIR spectroscopy. Figure 1.4.3 reports the absorbance spectra measured on the precursor

solution used for the MoS2 electrodeposition on FTO (left). Similar absorbance peaks are also seen in the electrodeposited MoS2 / FTO samples.

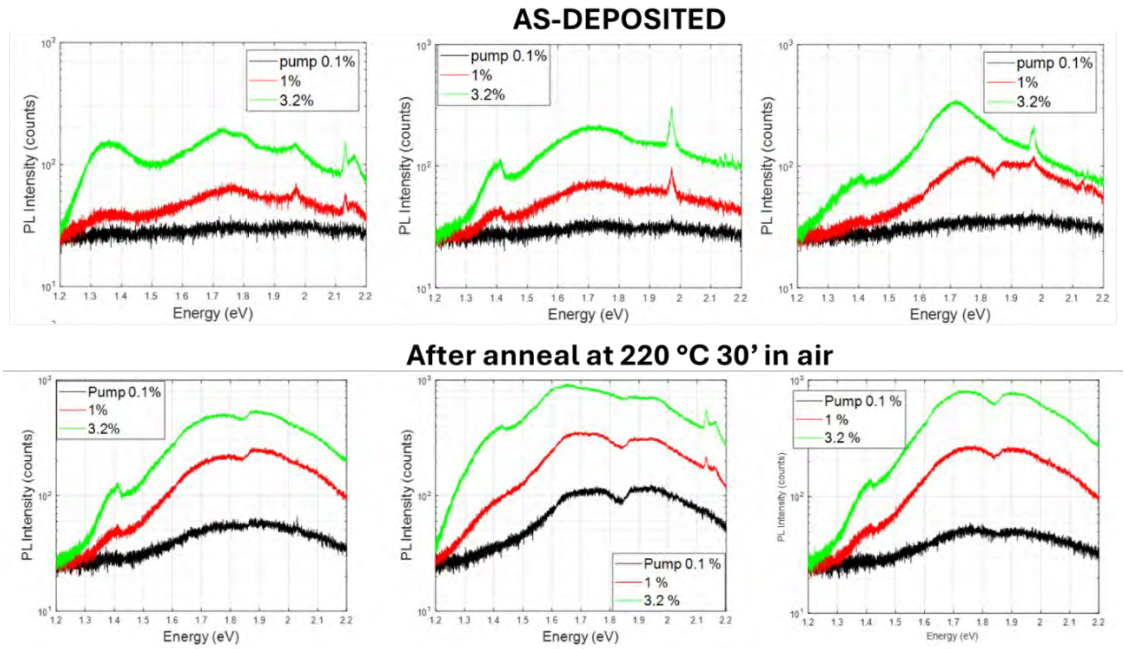

Figure 1.4.2. PL spectra of MoS2 / FTO Samples. Note the PL peaks in the energy range of about 1.7-2.1 eV, close to the MoS2 excitonic peaks observed in UV-VIS-NIR transmittance spectroscopy (see Fig. 1.4.3). Note also that the PL is much more intense in the annealed samples.

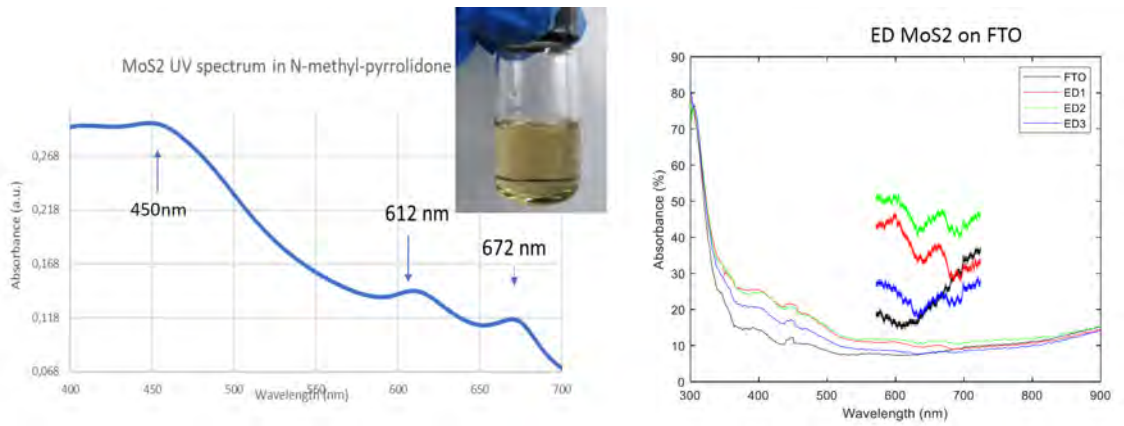

Figure 1.4.3. Absorbance spectra measured in the precursor solution used for the electrodeposition of MoS2 on FTO (left). Similar absorbance peaks are actually also seen in the electrodeposited MoS2 / FTO samples.

Nanofilms of MoS_2 and WS_2 were synthesized at RWTH Aachen University using the thermally activated conversion (TAC) method in a sulfur-rich environment. The Raman spectra of the synthesized materials show in Figure 1.4.4 characteristic peaks corresponding to the E_{2g} and A_{1g} vibrational modes, observed at 382 cm^{-1} and 407 cm^{-1} for MoS_2 and 352 cm^{-1} and 418 cm^{-1} for WS_2, respectively. The absorption spectra in Figure 1.4.4 further confirmed the presence of these materials through their distinct excitonic peaks: X_A and X_B at ~ 610 nm and ~ 660 nm for MoS_2, and ~ 515 nm and ~ 620 nm for WS_2. These results validated the successful synthesis of MoS_2 and WS_2 nanofilms, with their optical and vibrational properties aligning with the characteristic signatures of transition metal dichalcogenides.

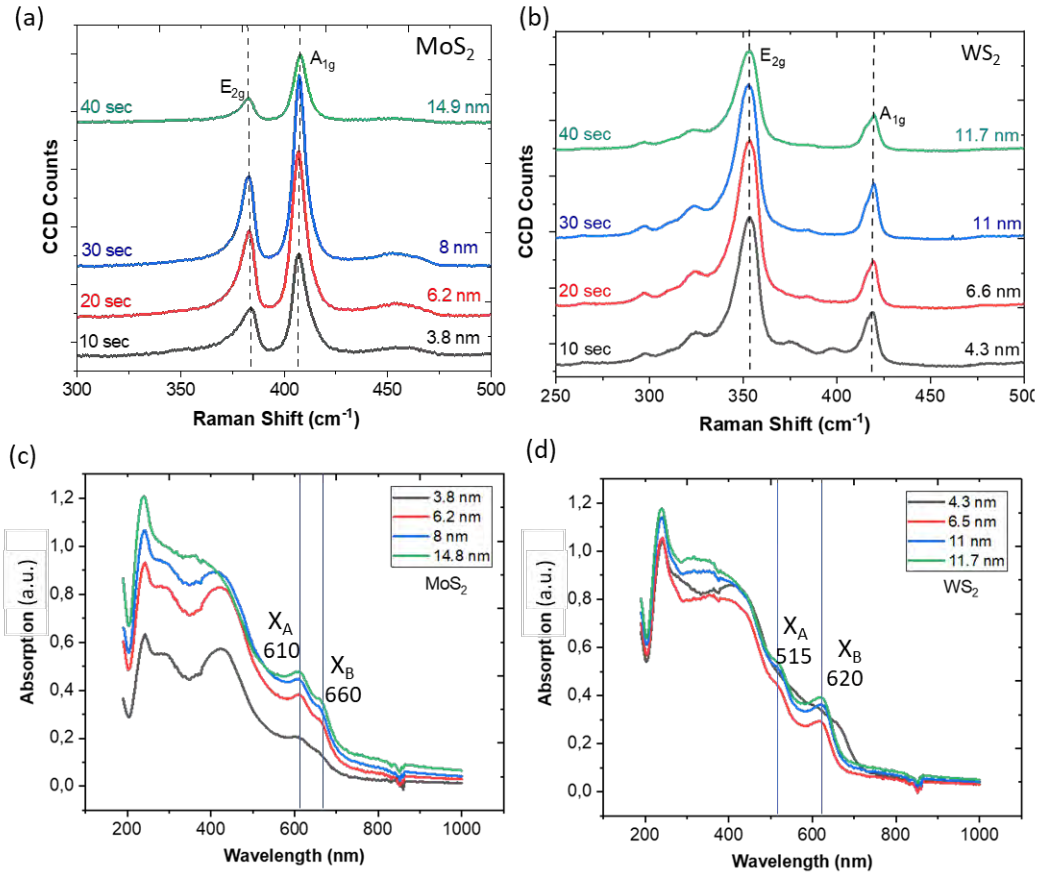

Figure 1.4.4: Raman (a,b) and absorbance spectra (c,d) with excitation peaks versus wavelength for the TAC MoS_2 and WS_2 at RWTH showing the characteristic MoS2 and WS2 signature.

AMO has grown TCO layers listed in Table 1.4.3 that provides the results from the Hall measurements for the TCO-4 and TCO-5 thin films carried out at UCC. The expected conductivity types were n-type for TCO-5 and p-type for TCO-4. It shows that TCO-5 is a good candidate both as an n-type junction material, as well as a TCO substrate.

Table 1.4.3: Hall measurements of single thin films from AMO, performed by UCC.

Sample	Sheet resistivity (Ω/sq.)	Resistivity (Ω*cm)	Sheet carrier concentration (cm^{-2})	Carrier concentration (cm^{-3})	Carrier type	Mobility ($cm^2/V*s$)
TCO-5 d1	394k	0.98	6.86×10^{13}	2.74×10^{19}	N (100%)	0.23
TCO-5 d2	821k	4.1	3.72×10^{13}	7.45×10^{18}	N (99%)	0.20
TCO-4 d1	269M	1.34k	failed	failed	failed	N/A
TCO-4 d2	599M	6k	failed	failed	failed	N/A

The Hall measurements on a single TCO-4 film were not successful, however an indirect measurement of TCO-4 was possible as part of a stack (bilayer structure). As the Hall effect electrical characterisation of these TCO-5/TCO-4 bilayers falls under Task 2.5, the results are presented there, but they do infer a p-type TCO layer influence, which is relevant here to the achievement of p-type TCOs.

Figure 1.4.5 shows UCC results with the G2V solar simulator photo-response under applied bias of -3 V for 0 % (NID, TMD-14), 5 % (TMD-21) and 18 % (TMD-25) Re-doped MoS2 TMDs

on c-cut sapphire with a ~7 nm TiO2 capping layer. A clear trend is observed of an increased photo-response with increased Re-doping in MoS2, indicating higher photo absorbance with doping.

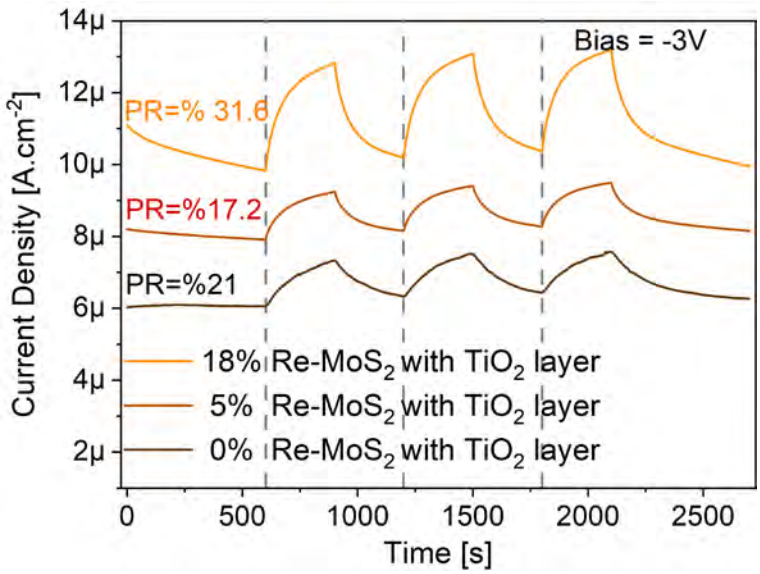

Figure 1.4.5: G2V photo-response under applied bias of -3 V for 0 % (NID, TMD-14), 5 % (TMD-21) and 18 % (TMD-25) Re-doped MoS_2 TMDs on c-cut sapphire with a ~7 nm TiO_2 capping layer. The response is to a G2V solar simulator light off/on sequence in time (off 600s, on 300s, off 300s, on 300s, off 300s, on 300s, off 600s). A clear trend is observed of an increased photo-response with increased Re-doping in MoS_2.

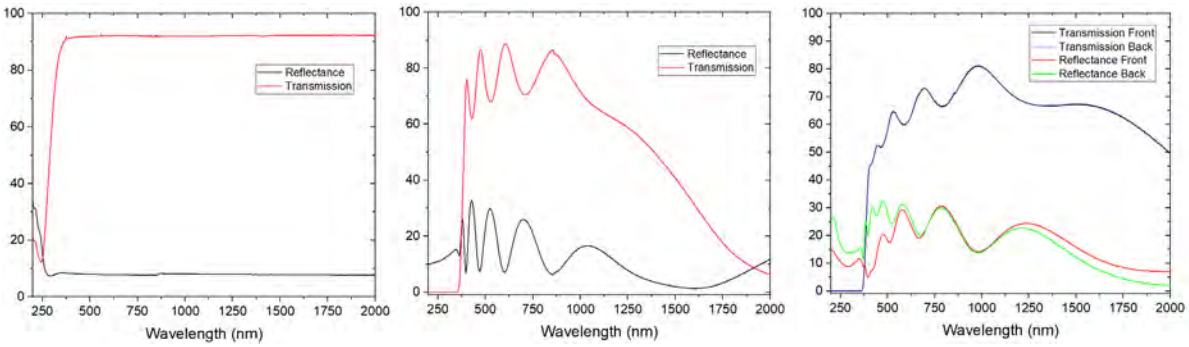

Figure 1.4.6: UV-Vis spectra (reflectance and transmission) of transparent glass (left), TCO-32 (centre) and TMD-06 on TCO-32 (right).

Work from AMO and UCC in Figure 1.4.6. shows the transmission and reflectance spectra, in a wide wavelength range from UV (200 nm) to infrared (2000 nm) light, of glass, TCO-32 and TMD-06 on TCO-32. Starting from a very transparent (>90 %) but electrically insulating glass (left), TCO-32 material was deposited by UCC while still retaining 70-90 % transparency for visible light (centre), and TMD-06 material on TCO-32 on glass (right). The reflectance peaks observed in the visible range are due to thin film interference and may enable back-reflection of light into the multi-layer system, thus increasing absorptance efficiency.

2. Task 1.5: Photoelectrochemical Characterisation of the TCOs and TMDs

2.1 Introduction

The objective of Tasks T1.5 in WP 1 is to photoelectrochemically investigate the TCO and TMD building block materials and their progress towards obtaining zero bias water splitting capability.

Importantly, increasing the area from small area PEC cells to large area PEC cells will assist in this objective, and we do see increasing large area capability.

2.2 Photoelectrochemical Results and Discussion

Photoelectrochemical activity is undertaken at UCC with a G2V Pico-Var Solar Simulator. We illustrate the spectrum for AM1.5G, 1.1 Suns (Effectively 0.9 x 1.1 Suns = 0.99 Suns due to ~10 % loss across window) in Figure 1.5.1. Inset is the NREL recorded spectra for AM 0, AM 1.5g and AM 1.5d. The G2V simulator uses 32 LEDs, giving a total radiance of 88.3mW/cm2 for a spectra of 361 - 1556 nm. A blackout dark chamber is employed to compare light off against light on measurements.

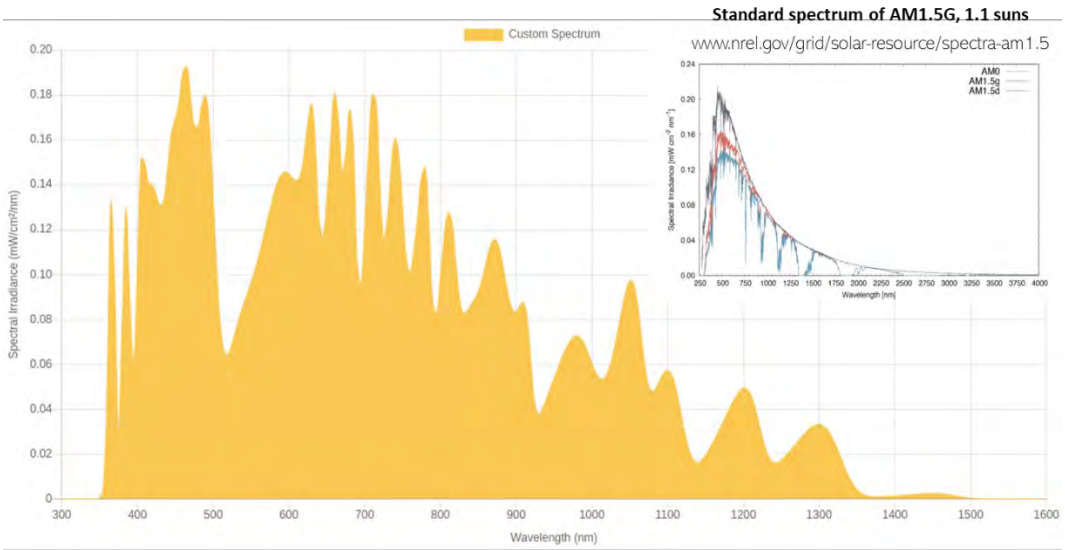

Figure 1.5.1: G2V Pico-Var Solar Simulator spectrum for AM1.5G, 1.1 Suns (Effectively 0.9 x 1.1 Suns = 0.99 Suns due to ~10 % loss across window). Inset is the NREL recorded spectra for AM 0, AM 1.5g and AM 1.5d. The G2V simulator uses 32 LEDs, giving a total radiance of 88.3mW/cm2 for a spectra of 361 - 1556 nm. A blackout dark chamber is employed to compare among others light off against light on measurements.

Figure 1.5.2 shows the G2V Photoelectrochemical response under -2.5 V applied bias with the solar simulator conditions specified in Figure 1.5.1 for 0 %, 5 % and 18 % Re-doped MoS2 and 0 % Nb-doped WS2 TMDs with a ~7 nm TiO2 capping layer. These preliminary diagnostic measurements showed a clear trend of an increased photocurrent response with increased Re-doping in MoS2.

For 0 % Nb-doped WS2 - while showing a decent photocurrent response, increased Nb-doping rapidly increased the conductivity towards semi-metal behaviour with a reducing photocurrent (not shown). When assessed in the context of the Hall-effect and TEM results, doped MoS2 is suitable for PEC cells, whereas WS2 is unsuitable due to poor doping modulation, mixing instability and W-W clustering.

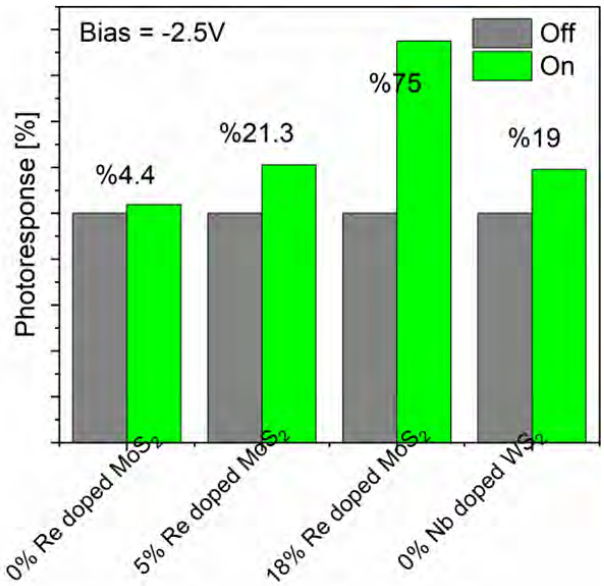

Figure 1.5.2: G2V Photoelectrochemical response under -2.5 V applied bias with the solar simulator conditions specified in Figure 1.5.1 for 0 % (TMD-15), 5 % (TMD-21) and 18 % (TMD-25) Re-doped MoS_2 and 0 % Nb-doped WS_2 (TMD-15) TMDs with a ~7 nm TiO_2 capping layer. These preliminary diagnostic measurements showed a clear trend of an increased photocurrent response with increased Re-doping in MoS_2. For 0 % Nb-doped WS_2 (TMD-15) - while showing a decent photocurrent response, increased Nb-doping rapidly increased the conductivity towards semi-metal behaviour with a reducing photocurrent (not shown). When assessed in the context of the Hall-effect and TEM results, doped MoS_2 is suitable for PEC cells, whereas WS_2 is unsuitable due to poor doping modulation, mixing instability and W-W clustering.

Figure 1.5.3 gives the PEC results for TCO-39. Photoelectrochemical (left) linear sweep voltammetry and (right) chronoamperometry responses under the conditions specified in the graphs. Water splitting is observed above a bias $\geqslant \pm$ 2.8 V, and a very low photocurrent is observed at zero bias.

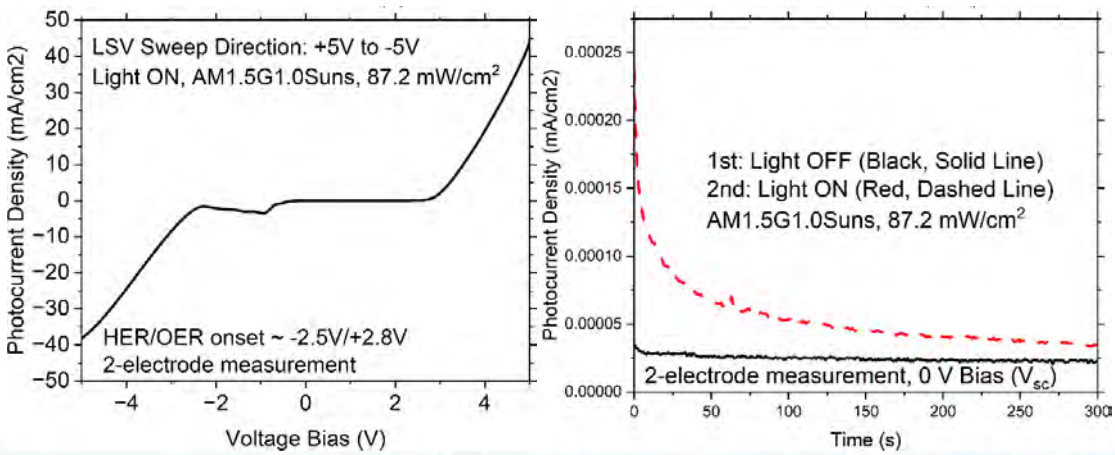

Figure 1.5.3: Sample TCO-39. Photoelectrochemical (left) linear sweep voltammetry and (right) chronoamperometry responses under the conditions specified. Electrolyte: 1 M ~ $K_3H_3P_2O_8$, ~ pH 7. A large area Pt counter electrode is employed. Water splitting is observed above a bias ≥ ±2-5-2.8 V, and a very low photocurrent is observed at zero bias.

When TCO-39 is replaced by TCO-32, we see the photocurrent density increasing at a lower voltage onset of ~1.5-2.0 V, although the current level is reduced significantly, which is important as there is no water splitting at that potential level. However, the zero bias photocurrent density is almost an order of magnitude higher than TCO-39. See Figure 1.5.4.

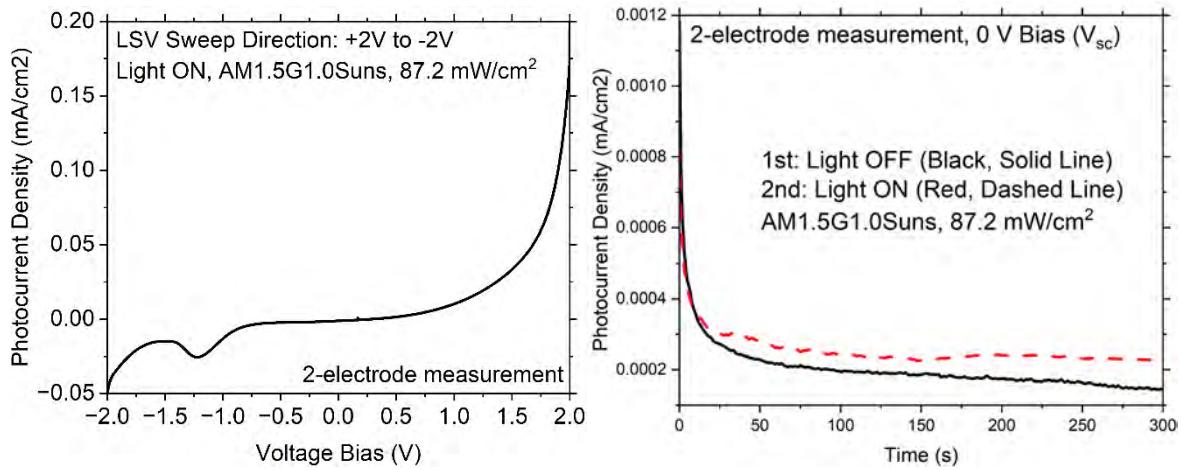

Figure 1.5.4: Sample TCO-32. Photoelectrochemical (left) linear sweep voltammetry and (right) chronoamperometry responses under the conditions specified. Electrolyte: 1 M ~ $K_3H_3P_2O_8$, ~ pH 7. A large area Pt counter electrode is employed. A rapid current increase is observed at ~1.5 V, and a very low photocurrent is observed at zero bias.

When TMD-06 is on TCO-32 with a TCO-14 capping and equivalently assessed, as in Figure 1.5.5 below, we see a significant order of magnitude increase in the photocurrent density at a similar voltage onset of ~1.5-2.0 V, but moving into the water splitting potential range. The zero bias photocurrent density is almost two orders of magnitude higher than TCO-32, which is very significant.

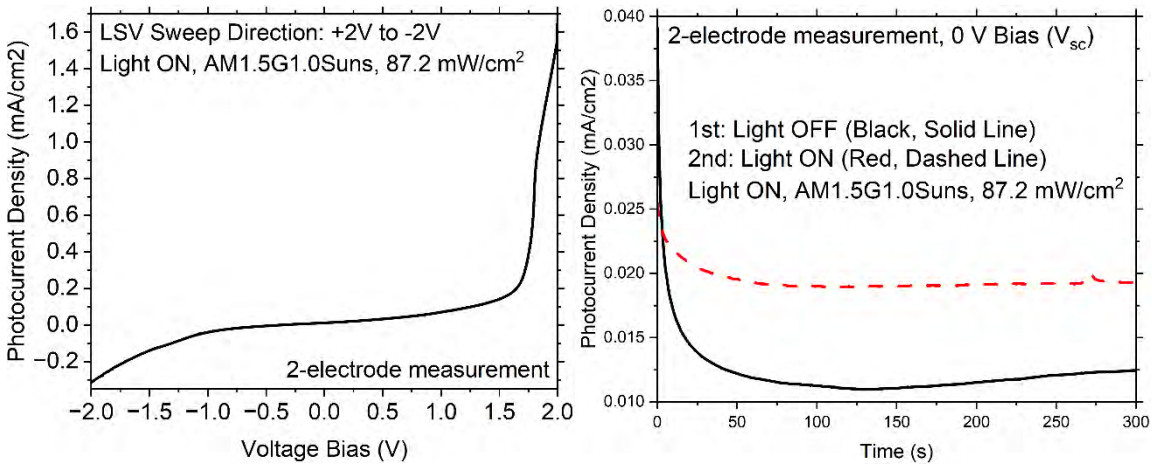

Figure 1.5.5: Sample TMD-06 on TCO-32 and capped by TCO-14. Photoelectrochemical (left) linear sweep voltammetry and (right) chronoamperometry responses under the conditions specified. Electrolyte: 1 M ~ $K_3H_3P_2O_8$, ~ pH 7. A large area Pt counter electrode is employed. A rapid photocurrent density increase is

observed at ~1.5-2.0 V that pushes the magnitude into the water splitting range, and a much higher photocurrent density is observed at zero bias.

These comparative results in Figures 1.5.3-1.5.5 for TCO-39, TCO-32 and TMD-06 on TCO-32 with a TCO-14 capping show that by replacing commercial TCO-39 firstly with our own developed TCO-32, we can at least improve the zero bias photocurrent density. However, by moving to a TMD-06 on TCO-32, we see a very significant boost to the photocurrent density by orders of magnitude, and importantly, pushing the photocurrent density further towards the water splitting level.

It can easily be inferred that by continued improvement to the TMD doping and to the TMD and TCO layers, and especially with increased numbers of TMD/TCO junctions alongside the observed area increases, the zero bias photocurrent density could potentially have a trajectory towards a water splitting capability.

3. Conclusions and Perspectives

Tables 0.1 (Task 1.1) and 0.2 (Task 1.2) list the building block TCO and TMD materials, respectively, investigated in WP 1 up to M26. The various physical, chemical and structural characterisation assessments in Task 1.3 confirm the formation of TCOs and TMDs.

The TCO-based activities in WP 1 included here in D1.3 are for the Task 1.4 electrical and optoelectronic characterisation of the building block TCOs and TMDs, as well as the Task 1.5 photoelectrochemical characterisation of the building block TCOs and TMDs. These provide possible options for the multijunction layers, for capping layers, and for use as a dedicated substrate. Significant understanding has been achieved for all of these objectives, and we have made significant progress towards advancing a usable substrate, potential capping layers, and the TCO layers for the multijunctions.

The TMD-based activities in WP 1 included here in D1.3 are for the Task 1.4 electrical and optoelectronic characterisation of the building block TCOs and TMDs, as well as the Task 1.5 photoelectrochemical characterisation of the building block TCOs and TMDs. Regarding TMD layers for multijunction absorber and pn-junction layers, significant understanding has been achieved regarding the influence of doping and other factors, such as resistivity, growth process, area, post-processing and substrate.

We conclude that the activities in WP 1 at M26 of the M40 timeline have produced material building blocks that show promise for a novel substrate, for capping layers, and for the TCO and TMD layers needed to realise the multijunction layered devices that could potentially reach the zero bias photocurrent density capability that pushes us into the water splitting regime.

Appendices

Appendix 1: List of acronyms

CVD	=	Chemical vapor deposition
DC	=	Direct current
PEC	=	Photoelectrochemical
PVD	=	Physical vapor deposition
RF	=	Radio frequency
TAC	=	Thermal Assisted Conversion
TCO	=	Transparent conductive oxide
TMD	=	Transition metal dichalcogenide
WP	=	Work Package